JACS
JOURNAL OF THE AMERICAN CHEMICAL SOCIETY
Article
pubs.acs.org/JACS

Quantum Dot Photoluminescence Quenching by Cr(III) Complexes. Photosensitized Reactions and Evidence for a FRET Mechanism

Peter T. Burks,[†,#] Alexis D. Ostrowski,[†,#] Alexander A. Mikhailovsky,[†] Emory M. Chan,[‡] Paul S. Wagenknecht,*[,†,§] and Peter C. Ford*[,†]

[†]Department of Chemistry and Biochemistry, University of California—Santa Barbara, Santa Barbara, California 93106-9510, United States

[‡]The Molecular Foundry, Lawrence Berkeley National Laboratory, Berkeley, California 94720, United States

[§]Department of Chemistry, Furman University, Greenville, South Carolina 29613, United States

Supporting Information

ABSTRACT: Reported are quantitative studies of the energy transfer from water-soluble CdSe/ZnS and CdSeS/ZnS core/shell quantum dots (QDs) to the Cr(III) complexes *trans*-$Cr(N_4)(X)_2^+$ (N_4 is a tetraazamacrocycle ligand, X^- is CN^-, Cl^-, or $\underline{O}NO^-$) in aqueous solution. Variation of N_4, of X^-, and of the QD size and composition allows one to probe the relationship between the emission/absorption overlap integral parameter and the efficiency of the quenching of the QD photoluminescence (PL) by the chromium(III) complexes. Steady-state studies of the QD PL in the presence of different concentrations of *trans*-$Cr(N_4)(X)_2^+$ indicate a clear correlation between quenching efficiency and the overlap integral largely consistent with the predicted behavior of a Förster resonance energy transfer (FRET)-type mechanism. PL lifetimes show analogous correlations, and these results demonstrate that spectral overlap is an important consideration when designing supramolecular systems that incorporate QDs as photosensitizers. In the latter context, we extend earlier studies demonstrating that the water-soluble CdSe/ZnS and CdSeS/ZnS QDs photosensitize nitric oxide release from the *trans*-Cr(cyclam)$(ONO)_2^+$ cation (cyclam = 1,4,8,11-tetraazacyclotetradecane) and report the efficiency (quantum yield) for this process. An improved synthesis of ternary CdSeS core/shell QDs is also described.

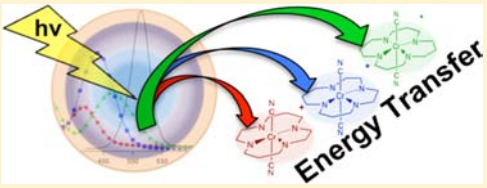

1. INTRODUCTION

A long-term goal of this laboratory is the development of polychromophore systems to release biologically active molecules such as nitric oxide for therapeutic applications upon single- or two-photon excitation.[1−3] NO is an endogenous bioregulator that plays important roles in vaso-relaxation, immune response, and tumor growth and suppression,[4−7] and may increase the effectiveness of γ-radiation treatment of hypoxic tumor tissue.[8] A very promising photochemical NO precursor is the chromium(III) complex *trans*-Cr(cyclam)$(ONO)_2^+$ (CrONO, cyclam = 1,4,8,11-tetraazacyclotetradecane).[9,10] However, CrONO's poor absorption cross section, especially at longer visible wavelengths, is a major drawback. Since QD single- and two-photon absorption cross sections are large,[11] we have been exploring the use of water-soluble semiconductor quantum dots (QDs) as antennas and have demonstrated the ability of such CdSe/ZnS core/shell QDs to sensitize CrONO photochemistry (Scheme 1).[10]

Understanding the mechanism of such photosensitization is essential to guide the design of new and more effective systems for potential applications. Although others have probed energy transfer from QDs to organic chromophores and other nanoparticles,[12] transition metal complex acceptors have received much less attention (see below).[13] The QD photosensitization of CrONO described above is accompanied by quenching of the QD "band-edge" photoluminescence (PL),

Scheme 1. Representation of NO Release from *trans*-Cr(cyclam)$(ONO)_2^+$ Using a CdSe/ZnS Core/Shell QD (Surface Modified with Dihydrolipoate) as a Photosensitizer

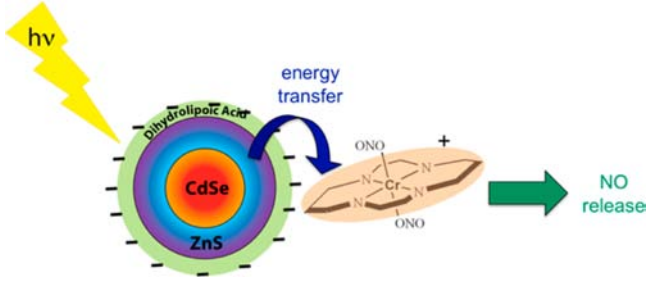

and we have suggested the associated processes to be the result of Förster resonance energy transfer (FRET) between the excited QD and CrONO cations assembled on the anionic surface.[10b] For the FRET mechanism, the rate constant for energy transfer from an excited state donor to an acceptor is predicted to be a function of the distance r (in Å) between the two chromophores and of the spectral overlap $J(\lambda)$ as shown in eq 1.[14]

Received: January 24, 2012
Published: July 18, 2012

$$k_{EN}(r) = \frac{C\Phi_{PL}\kappa^2}{\tau_{D(0)} r^6 n^4} J(\lambda) \quad (1)$$

where Φ_{PL} and $\tau_{D(0)}$ are the PL quantum yield and lifetime in the absence of acceptor, κ is the dipole−dipole orientation factor between the donor and acceptor ($\kappa^2 = 2/3$ for randomly oriented dipoles), C is a numerical constant, and n is the refractive index of the medium.

The present investigation was initiated to examine the energy transfer mechanisms between semiconductor QDs and metal complexes in solution by probing the effect of tuning the overlap integral $J(\lambda)$ of the donor emission and the acceptor absorbance. This can be accomplished by varying the size or composition of the QDs, which leads to shifts of the PL band and/or by varying the acceptor complexes. In this context, the present study examines QD PL quenching by three dicyano Cr(III) complexes *trans*-Cr(N_4)$(CN)_2^+$ (PF_6^- salts in each case), where N_4 = cyclam, isocyclam, and [16]aneN$_4$ (**1**, **2**, and **3**, Figure 1). These *trans*-Cr(N_4)$(CN)_2^+$ ions are photoinert,

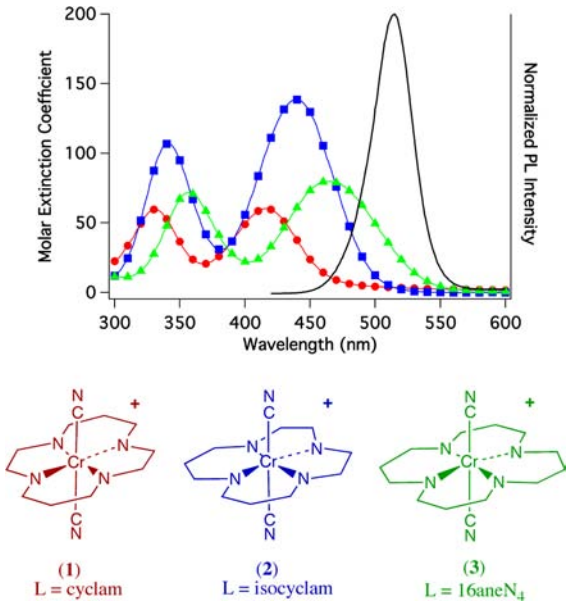

Figure 1. *trans*-Cr(N_4)$(CN)_2^+$ cationic complexes **1**, **2**, and **3** and their UV/vis absorption spectra: **1** (red dots), **2** (blue squares), and **3** (green triangles) in aqueous solution displaying metal-centered ligand field (d−d) transitions and their varied overlap with the PL from 515 nm-emitting CdSeS/ZnS core/shell QDs (see text).

not easily oxidized or reduced, and have analogous physical properties (size, charge, counterions). However, the modest differences in the N_4 macrocycles tune the average ligand field (LF) strengths following the order cyclam > isocyclam > [16]aneN$_4$, and this tunes the energies of their metal-centered, LF absorption band energies in the same order (Figure 1).[15] In turn, the overlap integrals between absorption spectra of the *trans*-Cr(N_4)$(CN)_2^+$ acceptors and the PL spectrum of a specific QD donor vary coherently and thus provide a more quantitative test of the FRET mechanism.

The ligand field absorption bands of the three dicyano Cr(III) complexes are all relatively high in energy,[15] so that bluer emitting QDs were desirable in order to achieve larger spectral overlaps. The PL quenching studies with this series of acceptors were therefore carried out using water-soluble cadmium selenide sulfide/zinc sulfide core/shell QDs, and the preparation and characterization of the ternary cores are described. Systematic studies on the effects of these dicyano complexes on the intensities and lifetimes of such QDs were carried out using two different, well-characterized sizes of these CdSeS/ZnS core/shell QDs, so that the effects of QD size and the corresponding PL energy on the spectral overlap with the three Cr(III) complexes could be quantitatively evaluated. In a similar context, we also describe studies evaluating QD size effect on the quenching by several *trans*-Cr(cyclam)X_2^+ (X^- = ONO^-, Cl^-, or CN^-) with water-soluble QDs having smaller sizes than previously reported. In addition, we follow up on the earlier study[10] of CdSe/ZnS core/shell QD photosensitized nitric oxide labilization from CrONO by measuring this process quantitatively.

2. EXPERIMENTAL SECTION

2.1. Cr(III) Compounds. The syntheses and purification of [*trans*-Cr(cyclam)$(CN)_2$]PF_6 (**1**), [*trans*-Cr(isocyclam)$(CN)_2$]PF_6 (**2**), [*trans*-Cr([16]aneN$_4$)$(CN)_2$]PF_6 (**3**) have been reported.[15]

2.2. Quantum Dot Synthesis and Characterization. The water-soluble CdSe/ZnS core/shell QDs with dihydrolipoic acid (DHLA) surface ligands used in this study were prepared using procedures based on those reported by Mattoussi et al.[16] The bluer emitting water-soluble ternary CdSeS/ZnS core/shell QDs with DHLA surface ligands were prepared via an adaptation of an earlier CdSeS synthesis[17] that we optimized using the robotic Workstation for Automated Nanocrystal Discovery and Analysis (WANDA) of the Molecular Foundry.[18] A detailed description of the resulting benchtop procedure and the WANDA optimization process leading to it are presented in the Supporting Information (Figures S-1 to S-4).

The size distributions of the CdSeS core and CdSeS/ZnS core/shell QDs were determined by transmission electron microscopy (TEM) using ultrathin carbon film/holey carbon on copper substrates with a Tecnai G2 F-20 S-Twin transmission electron microscope at 200 kV and 400k× magnification at the Suzhou Institute for Nanotech and Nanobionics in Suzhou, China. TEM-EDX data were obtained from six different locations on the grid and averaged to quantify the presence of Cd, Se, and S.

2.3. Photochemical Studies. The photoinduced release of NO from solutions of CrONO alone and of CrONO and water-soluble QDs together was determined using a General Electric model NOA-280i nitric oxide analyzer (NOA) under a flow of helium that carried the NO to the NOA. The integrated NOA signal gave a quantitative evaluation of the NO released, while the amount of light absorbed was calculated from the intensity of the light source, the absorbance of the solution at the excitation wavelength, and the irradiation time. The absorption spectra of the CrONO and QD solutions at the experimental concentrations were recorded to determine the amount of light absorbed by each component. Direct photolyses of analogous solutions of CrONO alone were studied in order to determine the NO generated by the unsensitized photoreactions. All CrONO solutions were prepared fresh each day and stored in the dark until used.

2.4. Steady State Photoemission Measurements. Optical studies were performed in 1 cm path length quartz cells. Electronic absorption spectra were recorded on a Shimadzu dual beam UV-2401 PC spectrophotometer, while photoluminescence spectra were recorded using a Photon Technology International (PTI) fluorimeter at 1 nm resolution with a model 814 PMT detector. Emission quantum yields were measured using the method of Crosby and Demas[19] with Rhodamine 6G (0.95 in ethanol) as the standard.

Quenching experiments under continuous excitation were performed with several core/shell QD preparations having different emission maxima. The QD stock solutions were prepared by diluting concentrated water-soluble QD solutions with pH 7.9 phosphate buffer solution (15 mM) to give an exciton absorbance between ~0.30 and 0.60, and experiments using that solution were performed in a single day. Stock solutions of the quenchers were prepared by dissolving ~5 mg of the Cr(III) salt in 5 mL of pH 7.9 phosphate

dx.doi.org/10.1021/ja300771w | J. Am. Chem. Soc. 2012, 134, 13266−13275

buffer solution (15 mM) with exact concentrations determined from the absorption spectra and extinction coefficients.[15b] Solutions for quenching experiments were prepared by adding different volumes of a Cr(III) stock solution and sufficient buffer to give 2.9 mL total volume. A 100 μL sample of the QD stock solution was then added to the 1.0 cm quartz cuvette leading to a 30× dilution and QD concentrations in the range 30−50 nM. The UV/vis absorption spectrum was recorded immediately. The PL spectrum was then measured at two excitation wavelengths, the minimum absorption of the quencher compound and at 310 nm. All PL measurements were carried out at 20 °C using a controlled temperature cuvette holder (10 min equilibration time). Reported PL intensities were corrected for modest inner filter effects due to quencher absorption of excitation light and of the QD emission. This was done by assuming an average path length of 0.5 cm (PL detection was at 90°), converting the quencher absorption at the specified wavelength to transmittance, and then correcting the QD PL intensity accordingly.

2.5. Time-Resolved PL and Transient Absorption Experiments. Stock solutions of QD and Cr(III) quencher were prepared immediately before the planned experiment as described above. Care was taken to ensure that contact time between the quencher and QD was the same for all samples. Temporal emission decay measurements were carried out at the UCSB Optical Characterization Facility using the time-correlated single-photon-counting technique.[10b] The excitation wavelength was 400 nm, and the instrument response was ~70 ps. Transient absorption studies were performed similarly, although solution concentrations were scaled to improve the signal.

3. RESULTS AND DISCUSSION

As noted in the Introduction, an earlier study[10] demonstrated that DHLA-treated CdSe/ZnS core/shell QDs (PL λ_{max} 570 nm) photosensitize NO release from the Cr(III) complex *trans*-Cr(cyclam)$(ONO)_2^+$ (Scheme 1) when excited with polychromic light in pH 7.9 buffered solutions. The PL from these QDs (3.8 nm CdSe cores) was quenched in a concentration-dependent manner by CrONO and by the analogous dichloro cation *trans*-Cr(cyclam)Cl_2^+ (**4**) but not by *trans*-Cr(cyclam)-$(CN)_2^+$ (**1**). Given that the absorption spectra of **4** and of CrONO overlap with the 570 nm PL but the spectrum of **1** does not (see Figure S-5, SI), FRET appeared to be the likely quenching mechanism, although there were quantitative aspects that needed to be probed more critically. In the same study, it was also shown that adding KCl (250 mM) decreased by ~5-fold the effective quenching by **4**, whereas the PL intensity from the same CdSe/ZnS core/shell QDs without added **4** was unaffected by KCl up to 1 M. On this basis, we argued that PL quenching (as well as photosensitized NO release from CrONO) occurs in electrostatic assemblies formed by ion pairing between the Cr(III) complex cations and the QD surfaces, which are anionic (and therefore water-soluble) owing to the DHLA carboxylate groups at this pH (Scheme 2). The K^+ ions compete with Cr(III) cations for the ion pairing sites on the QD surface, hence decreasing the effectiveness of quenching by the latter cations.

3.1. Photosensitization and Photophysical Studies with CdSe/ZnS Core/Shell QDs. The experiments described in this section involve DHLA surface-modified, water-soluble CdSe/ZnS core/shell QDs with a PL λ_{max} of 536 nm and core diameters estimated according to Mikulec et al.[20] as 2.8 nm. As noted, the analogous QDs used in the earlier study had a PL λ_{max} of 570 nm and estimated core diameters of 3.8 nm.

Photosensitization. Reported here are experiments quantifying the photosensitization of NO release by such QDs. Figure 2 depicts the signals displayed by the Sievers nitric oxide analyzer (NOA) upon 436 nm irradiation of aqueous solutions

Scheme 2. Suggested Destabilization of QD/Cr(cyclam)X_2^+ Electrostatic Assemblies in the Presence of High Concentrations of Added KCl

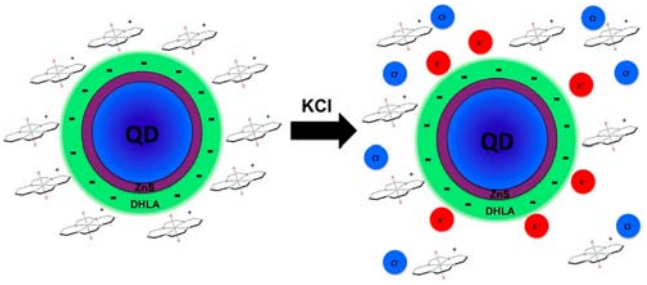

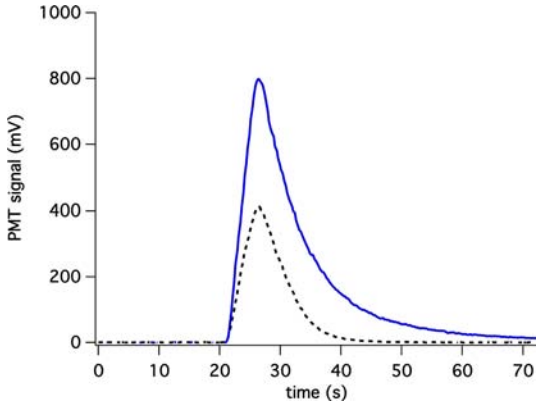

Figure 2. Comparison of NOA signals indicating NO release following 5 s irradiation (at 436 nm) of CrONO (400 μM) in pH 7.4 phosphate buffer solutions (15 mM) under flowing He with (solid blue line) and without (dashed black line) added CdSe/ZnS core/shell QDs (400 nM). The QDs displayed a band-edge emission λ_{max} at 536 nm with 2.8 nm estimated core diameters. The integrated areas of these signals correspond to the amount of NO released (1.6 nmol with QDs present; 0.5 nmol with only CrONO).

containing CrONO. The solutions are continuously swept with helium, and the integrated NOA signal determines the total NO generated during the photolysis interval. The CrONO concentration was 400 μM in each case, but the one showing the higher NO production also contained 400 nM of these QDs (PL λ_{max} of 536 nm). As seen before with larger CdSe/ZnS core/shell QDs,[10b] the QDs dramatically increase the photolysis-induced NO generation. Since light absorption by the latter solution is largely by the QDs, the ~3× enhanced NO production is attributed to a mechanism by which QD excitation sensitizes NO formation from the CrONO cations associated with the nanoparticle surface.

The quantum yield of NO photoproduction (Φ_{NO}, defined as moles of NO released per Einstein of light absorbed) upon direct 436 nm excitation of CrONO in aqueous buffer solutions was previously measured as 0.25 ± 0.03.[9c] The Φ_{NO} is essentially independent of the excitation wavelength (λ_{irr}) in the visible leading to the suggestion that the photoactivity can primarily be attributed to the lowest energy doublet and quartet excited states of the *trans*-Cr(cyclam)$(ONO)_2^+$ cation.[9b,c] In contrast, the overall efficiency of NO release attributed to the light directly absorbed by the QDs was a much lower 0.05 ± 0.01. This was expected, since the actual quantum yield for sensitized NO release Φ_{Sen} would be the product of energy transfer from sensitizer to acceptor (Φ_{en}) times Φ_{NO} (eq 2). Since Φ_{NO} = 0.25, Φ_{en} under these conditions would be 0.20 ±

dx.doi.org/10.1021/ja300771w | J. Am. Chem. Soc. 2012, 134, 13266−13275

0.04. This correlates reasonably with the amount of PL quenching (~16%) for an analogous 400 nM QD (536 nm PL) solution containing 360 μM CrONO.

$$\Phi_{Sen} = \Phi_{en} \times \Phi_{NO} \quad (2)$$

We have used the NOA to examine the enhanced production of NO from dilute solutions of CrONO (100 μM) without added QDs and in the presence of water-soluble CdSe/ZnS core/shell QDs (700 nM, PL λ_{max} 536 nm) or of the CdSeS/ZnS core/shell QDs (100−250 nM, PL λ_{max} 484 or 515 nm) utilized in the quenching studies described below. In each case the solution was pH 7.9 phosphate buffer (15 mM), and several different excitation wavelengths were probed. The emission intensities of these solutions were also recorded for the identical conditions. Fresh solutions were prepared for each measurement, owing to the discovery that the CrONO photoproduct itself is a strong quencher.

No NOA signal was observed from QD solutions when CrONO was not present or at excitation wavelengths >550 nm, where the solutions did not absorb light. At the other visible/near-UV excitation wavelengths, the presence of quantum dots enhanced the photoinduced production of NO regardless of which QD was present, and the presence of CrONO led to quenching of the QD PL at magnitudes consistent with level of NO production. This coincidence of NO production and PL quenching supports the conclusion that the QDs are acting as antennae to photosensitize NO release from CrONO, as was described above. The greatly enhanced absorbances of the CrONO/QD solutions thus make them much more effective in collecting the incident light and, correspondingly, enhance the rates of NO production. Notably for excitation wavelengths less than 300 nm, we found that the NO production from CrONO/QD solutions as well as the PL efficiency from solutions of QDs alone both decreased, the latter phenomena having been observed previously.[21]

In the discussion above, the enhanced NO formation is assumed to be the result of energy transfer from QD antennas to CrONO. This view has its origin in the earlier studies with 570 nm PL CdSe/ZnS core/shell QDs, where it was noted that spectral overlap appeared to be a requirement for PL quenching, and from the present studies where quenching of the PL from three other QD sets shows similar behavior. Others have reported FRET pathways for energy transfer between QDs and various dyes at the surface,[12a] including Ru(II) bipyridine derivatives.[13d] Among the experimental studies supporting this mechanism was the fit of the quenching efficiency of certain QD−dye conjugates to the r^{-6} relationship described by eq 1.[12a] However, charge transfers (CT) between excited CdSe QDs to and/or from various substrates at the surface are also known quenching pathways,[13a−d,f] so a CT mechanism must be considered for CrONO as well.

For example, other QD−Ru(II) complex conjugates have been shown to undergo quenching via hole transfer from the valence band of the excited QD,[13a,b,e] leading to substrate oxidation. Would such oxidation of CrONO lead to NO formation? This was tested by using the NOA to evaluate NO production from an aqueous CrONO solution upon addition of aliquots of Ce(IV) solution (aq ceric ammonium nitrate). The NOA gave no evidence of nitric oxide generation even when sufficient Ce(IV) was added to destroy the CrONO completely (to unknown products). In contrast, merely shining a flashlight on the CrONO solution was sufficient to trigger a strong signal from the NOA. CT in the opposite direction, namely electron transfer to the Cr(III) substrate is unlikely, owing to the very unfavorable reduction potential[10] of CrONO although it has been documented for more easily reduced substrates such as $Re(CO)_3Cl(dcbpy)$ (dcbpy = 4,4′-dicarboxy-2,2′-bipyridine).[13f] On these bases, we conclude that the QD photosensitized NO release from CrONO and the associated quenching of QD PL are largely due to an energy transfer rather than a CT mechanism.

Quenching of PL from the Smaller Water-Soluble CdSe/ZnS Core/Shell QDs by trans-Cr(cyclam)X_2^+. For the larger quantum dots, the PL (λ_{max} 570 nm) overlapped with the lowest energy, spin-allowed d−d absorptions of CrONO (λ_{max} 480 nm) and of *trans*-$Cr(cyclam)Cl_2^+$ (**4**, λ_{max} 570 nm) but not with that of *trans*-$Cr(cyclam)(CN)_2^+$ (**1**, λ_{max} 420 nm). Consistent with a FRET mechanism, quenching was observed for CrONO and for **4**, but not for **1**. For the smaller CdSe/ZnS core/shell QDs having a PL λ_{max} of 536 nm, the PF_6^- salts of CrONO, **4**, *and* **1** all quenched the QD PL, with **1** now being about as effective as **4**, as expected owing to enhanced overlap with the former and decreased overlap with the latter. Interestingly, for both sets of QDs, CrONO was the strongest quencher, despite having a smaller spectral overlap with the larger QDs than did the dichloro analogue **4**. However, under these conditions CrONO is simultaneously undergoing photoreaction, so the nature of the species at the QD surfaces is changing progressively. Furthermore, the products formed by exhaustive photolysis are more effective quenchers than CrONO itself (see Figure S-6, SI), thus making a quantitative comparison of quenching by this complex to that by other *trans*-$Cr(cyclam)X_2^+$ cations challenging. For this reason we concluded that a more systematic set of photoinert acceptors was needed to explore the quenching mechanism, and this led to the following study with the three dicyano complexes (Figure 1) and bluer emitting ternary CdSeS QDs.[22,23]

3.2. Studies with Water-Soluble CdSeS/ZnS Core/Shell QDs. *Synthesis and Characterization.* The ternary CdSeS cores were prepared by a benchtop procedure developed following the WANDA optimization of key variables as described in the SI. With this method, one can reproducibly obtain CdSeS cores with PL maxima between ~450 and ~510 nm, the λ_{max} being a function of the reaction time allowed (Figure 3).

QD size distributions were determined by TEM, measuring >100 individual nanoparticles from different regions of the grid. In this manner, average diameters of 2.6 and 2.8 nm were determined for the 477 and 511 nm emitting CdSeS cores, respectively, while the 474 and 515 nm PL water-soluble CdSeS/ZnS core/shell QDs gave average diameters of 3.1 and 3.7 nm, Figure S-7 (SI). Given a calculated ZnS monolayer thickness of 0.31 nm,[24] the respective ZnS shells would appear to be roughly 1 to ~1.5 monolayers. The ZnS shells significantly increased emission intensity and reduced trap emission in both sets of QDs. EDX spectroscopy of the 477 and 510 nm PL CdSeS cores gave the respective Cd/Se/S relative compositions 1.00:0.79:0.16 and 1.00:0.57:0.37. The PL spectra of the 515 and 474 nm PL water-soluble CdSeS/ZnS core/shell QDs used in the studies described here are shown in Figures 1 and S-8 (SI), respectively, while the absorption spectra of the two are shown in Figure S-9 (SI).

Emission Quantum Yields. The PL quantum yields were measured in pH 7.9 phosphate buffer solution (15 mM) by comparison to Rhodamine 6G.[19] The values obtained in this

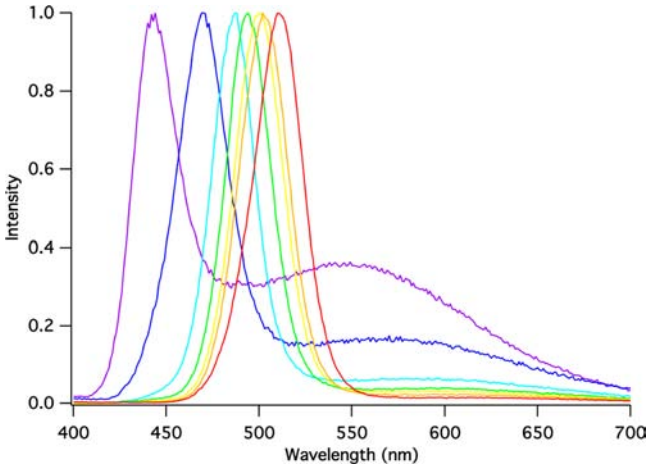

Figure 3. Normalized PL of aliquots removed at different times from the CdSeS QD benchtop synthesis as described in the SI. Over 10 min, the band-edge PL λ_{max} shifts from 444 to ~510 nm, while the full width at half maximum (fwhm) varies between 1180 and 1611 cm^{-1} (146−200 meV).

manner were 0.11 for the 515 nm PL core/shell QDs and 0.21 for the 474 nm PL core/shell QDs.

Quenching Studies. The studies here were designed to probe the effect of spectral overlap on quenching of QD PL. $J(\lambda)$ can be calculated using eq 3,

$$J(\lambda) = \frac{\int F_D(\lambda)\varepsilon_A(\lambda)\lambda^4 \, d\lambda}{\int F_D(\lambda) \, d\lambda} \quad (3)$$

where $F_D(\lambda)$ is the corrected PL intensity at wavelength λ (in nm), and $\varepsilon(\lambda)$ is the acceptor extinction coefficient at that λ. As noted above, the *trans*-$Cr(N_4)(CN)_2^+$ cations **1**, **2**, and **3** (N_4 = cyclam, isocyclam, and [16]aneN$_4$, respectively) display differences in average ligand field (LF) strengths following the order **1** > **2** > **3**. Thus, the characteristic longer wavelength, quartet LF absorption bands shift from higher to lower energy across this series. For a set of monodisperse quantum dots, the spectral overlap between the LF absorption and the QD PL varies systematically with N_4 as illustrated by Figure 1 for the core/shell QDs with PL centered at 515 nm and by Figure S-8 (SI) for those with PL centered at 474 nm. We can also assume that approximately the same number of these Cr(III) cations will associate with the anionic surface of a particular size QD for a specific Cr(III) concentration (see below). Thus, the extent of quenching can be compared to the spectral overlap as calculated by eq 3 to see if there is the correlation predicted by the FRET mechanism.

Table 1 summarizes the integrated overlap integrals of the PL bands for sets of water-soluble CdSeS/ZnS core/shell QDs having PL centered at 474, 484, and 515 nm with the absorption spectra of the dicyano Cr(III) complexes calculated using eq 3. The spectral overlap in each case follows the order **3** > **2** > **1**. The *relative* changes are greater for the larger QDs, although the *absolute* values of $J(\lambda)$ are considerably smaller.

Steady State PL and Quenching. The change in QD photoluminescence intensity was measured using seven different concentrations of each *trans*-$Cr(N_4)(CN)_2^+$ salt for both water-soluble CdSeS/ZnS core/shell QD samples. Notably, the added Cr(III) quenchers did not affect the QD absorption spectra. Figure 4 shows representative changes in the experimental emission spectrum observed for quenching of

Table 1. Calculated Overlap Integrals $J(\lambda)$ between the Absorption Spectra of the *trans*-$Cr(N_4)(CN)_2^+$ Complexes with N_4 = Cyclam, Isocyclam or [16]aneN$_4$ (1, 2, or 3, Respectively) and the PL Spectra of CdSeS/ZnS Core/Shell QD Preparations with λ_{max}^{em} Values at 474, 484, and 515 nm in Aqueous Solution[a]

	$J(\lambda)$ (in M^{-1} cm^{-1} nm^4)		
	1	**2**	**3**
515 nm PL QDs	1.8×10^{11}	6.6×10^{11}	2.2×10^{12}
(normalized to **1**)	1.0	3.6	12.2
484 nm PL QDs	3.3×10^{11}	2.3×10^{12}	3.2×10^{12}
(normalized to **1**)	1.0	6.9	9.8
474 nm PL QDs	4.4×10^{11}	3.1×10^{12}	3.4×10^{12}
(normalized to **1**)	1.0	6.9	7.6

[a]The spectral window was 420−600 nm.

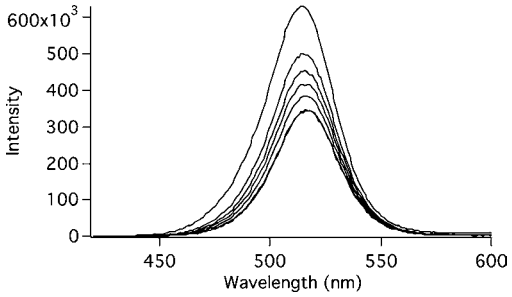

Figure 4. Decreases in the emission intensity from the 515 nm PL QDs in the presence of increasing concentrations (100−1000 μM) of **3**. There is a slight red-shift (1−2 nm) and narrowing (~2 nm) of the PL band at higher [**3**].

the 515 nm PL QDs by **3**, and the full data set is shown in Figures S-10 and S-11 (SI). Changes in the emission intensity (corrected for inner filter effects on excitation and PL) are shown in Figure 5 as plots of I^0/I, where I^0 is the PL intensity at the λ_{max} in the absence of any added Cr(III) complexes and **I** is the PL intensity when a particular concentration of the quencher was added. The resulting plots are not linear, as would be expected for bimolecular dynamic quenching. Instead they level off at higher [q] consistent with saturation of the anionic QD surfaces owing to ionic pairing with the cationic Cr(III) complexes. Nonetheless, two qualitative trends are clear. First, **1**, **2**, and **3** are each more effective in quenching the PL from the 474 nm QDs than in quenching the PL from the 515 nm emitting QDs. Second, for both QD preparations, quenching effectiveness follows the order **3** > **2** > **1**.

The latter observation clearly follows the trend for the calculated overlap integrals as summarized in Table 1. The trend with regard to quantum dot size is also as expected, since the spectral overlap of the three Cr(III) cations with the 474 nm PL QDs is larger in each case than with the 515 nm PL QDs. In addition, the smaller diameters and somewhat thinner ZnS shell for the 474 nm PL QDs may also play roles given the r^{-6} dependence of energy transfer rates (eq 1).

The quenching of a third set of CdSeS/ZnS core/shell quantum dots with a PL λ_{max} at 484 nm by systematically varied concentrations of **1**, **2**, and **3** was also probed. In this case, TEM data regarding the average size and size distribution were not obtained owing to insufficient material; however, given the synthesis procedure and the PL λ_{max}, it is reasonable to assume that these QDs are intermediate in size between the two

dx.doi.org/10.1021/ja300771w | J. Am. Chem. Soc. 2012, 134, 13266−13275

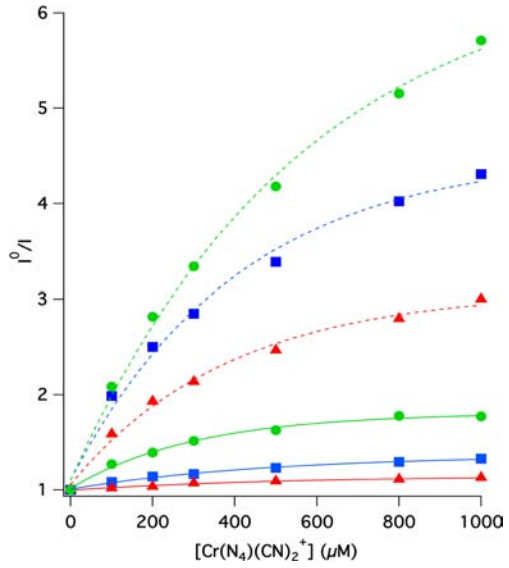

Figure 5. (*Solid lines*): Plots of $\mathbf{I^0/I}$ for quenching of the 515 nm PL QDs versus concentration by **1** (red triangles), **2** (blue squares), and **3** (green circles). (*Dashed lines*): Analogous plots for quenching of the 474 nm PL QDs by **1** (red triangles), **2** (blue squares), and **3** (green circles). In all cases the excitation wavelength was 310 nm. The **I** values have been corrected to compensate for inner filter effects from the Cr(III) complexes both on excitation and on the QD PL.

described above. Again the spectral overlap with the dicyano complexes follows the order **3** > **2** > **1** (Table 1) as does the pattern of concentration-dependent PL quenching (Figure S-12, SI). Furthermore, for any one Cr(III) complex (as illustrated in Figure S-13, SI), the pattern noted above that the smaller QDs are more effectively quenched is followed, presumably because of the greater spectral overlap as well as the shorter distance between the donor and acceptor chromophores.

In order to model this system, we will make several assumptions. First, given the analogous structures of **1**, **2**, and **3**, these cations should have similar association constants with the anionic QD surface. Second, for a particular quencher (**1**, **2**, or **3**), the total rate constant for energy transfer, k_Q(total), is additive, as has been assumed by others,[13d]

$$k_Q(\text{total}) = nk_q(i) \tag{4}$$

where n is the number of *trans*-$Cr(N_4)(CN)_2^+$ cations assembled on the QD surface and therefore is a function of the quencher concentration, and $k_q(i)$ is the unimolecular rate constant for static quenching by a single cation of quencher i at the surface. Clearly, the value $k_q(i)$ depends on the identities both of the quencher (i) and of the QD (j). The third assumption would be that a QD of a particular size has a single lifetime $\tau^0(j)$, where j denotes the specific QD sample. Given these simplified assumptions, it can be shown that the experimental ratios $\mathbf{I^0/I}$ in Figure 5 would be

$$\mathbf{I^0/I} = 1 + \tau^0(j) \times k_Q(\text{total}) \tag{5}$$

where k_Q(total) is defined by eq 4. Thus, if we assume n is independent of whether the cation is **1**, **2**, or **3**, then k_Q(total) should scale with the overlap integral (within a single QD sample) if FRET is the dominant mechanism. Using this model, one can calculate the *relative* values of k_Q(total) from the data for each quencher concentration $[q]$. Take, for example, the data for the 515 nm PL QDs. The relative k_Q(total) values are 1.0, 3.8, and 10.6 for 200 μM **1**, **2**, and **3**, and 1.0, 2.7, and 6.0 for 1.0 mM **1**, **2**, and **3**, respectively. These compare quite favorably to the relative spectral overlaps of 1.0, 3.6, and 12.2 reported in Table 1. If we examine the analogous data for the 474 nm PL QDs, the qualitative trend holds. The relative k_Q(total) values are 1.0, 1.7, and 2.4 for 1.0 mM **1**, **2** and **3**, respectively, while the calculated relative spectral overlaps are 1.0, 6.9, and 7.2. Although in both cases the experimental trends are somewhat attenuated versus the differences in $J(\lambda)$, it is clear that spectral overlap is important, suggesting that a FRET mechanism plays a major role in defining the quenching rates.

The association of the Cr(III) cationic complexes (q) with the anionic surface of the water-soluble QDs presumably involves serial equilibria as illustrated in Scheme 3. The binding constants $K_q^{(k)}$ should progressively decrease with each q associated with the QD to a maximum number m, where the surface is saturated.

Scheme 3. Serial Equilibria for Association of Quenchers q with the QDs up to a Maximum Number m

$$\text{QD} + q \rightleftharpoons \text{QD(q)} \qquad K_q^{(1)}$$

$$\text{etc to}$$

$$\text{QD(q)}_{m-1} + q \rightleftharpoons \text{QD(q)}_m \qquad K_q^{(m)}$$

For the above model, eq 5 can be rewritten as eq 6 where n is the only term dependent on $[q]$.

$$\mathbf{I^0/I} = 1 + \tau^0(j)nk_q(i) \tag{6}$$

Although the sequential $K_q^{(k)}$ values are unknown, from an operational perspective it is notable that curves drawn through the $[q]$-dependent data in Figure 5 were obtained empirically by fitting the $\mathbf{I^0/I}$ values to the exponential function

$$\mathbf{I^0/I} = f([q]) = 1 + c(1 - e^{-b[q]}) \tag{7}$$

where the quencher concentration $[q]$ is in μM, and b and c are constants for a specific QD j. Comparison of eqs 6 and 7 gives $c = \tau^0(j)\ k_q c'$, where $c' = n(1 - e^{-b[q]})^{-1}$. Furthermore, we suggest that c' equals m, the maximum number of q's that occupy the surface when saturated at high $[q]$. Values of c and b are listed in Table 2; other details are summarized in the SI.

If one assumes hexagonal closest packing of q on the QD surfaces, then m can be estimated from the equation: $m = 3.76(r_{QD}/r_q)^2$, where r_{QD} is the QD radius and r_q is the radius of q

Table 2. Parameters Used To Fit the I^0/I Data of Figure 6 to the Function $I^0/I = 1 + c(1 - e^{-b[q]})$

	c	b	$10^2\ c/m^a$	c/m normalized to **1**
515 nm PL QDs				
q = **1**	0.15	0.0019	0.18	1.0
q = **2**	0.36	0.0020	0.44	2.4
q = **3**	0.79	0.0033	0.97	5.4
474 nm PL QDs				
q = **1**	2.0	0.0026	3.1	1.0
q = **2**	3.4	0.0024	5.2	1.7
q = **3**	5.5	0.0018	8.4	2.7

[a] m calculated as described in the text as ~65 and ~81 for the 474 and 515 nm PL QDs, respectively.

dx.doi.org/10.1021/ja300771w | J. Am. Chem. Soc. 2012, 134, 13266−13275

(see SI). The r_{QD} values were estimated as 2.55 and 2.85 nm for the 474 and 515 nm PL QDs, respectively, on the basis of core/shell diameters determined by TEM studies, plus an estimated 1 nm layer of surface ligands, primarily the DHLA anions. The r_q was estimated as 0.615 nm on the basis of DFT calculations of the $Cr(N_4)(CN)_2^+$ cations plus an assumed hydration sphere for each ion.[25] Accordingly, m values of ~65 and ~81 were calculated for the 474 and 515 nm PL QDs, respectively. Thus if $c' = m$, the term c/m listed in Table 2 represents the relative values of k_q for the specific conditions and quencher. Notably, this ratio follows the sequence **3** > **2** > **1** reflecting the trend in spectral overlap.

Time-Resolved Photoluminescence (TRPL). Three sets of experiments were designed to evaluate the TRPL using the ultrafast spectroscopic techniques of the UCSB Optical Characterization Facility:

(1) Temporal emission at the PL λ_{max} from a fixed concentration (30 nM) of the 474 nm PL CdSeS/ZnS (core/shell) QDs alone and with 500 μM each of **1**, **2**, or **3** as the PF_6^- salts.
(2) Temporal emission at the PL λ_{max} from a fixed concentration (50 nM) of the 515 nm PL CdSeS/ZnS (core/shell) QDs alone and with 500 μM each of **1**, **2**, or **3** as the PF_6^- salts.
(3) Temporal emission at the PL λ_{max} from a fixed concentration (50 nM) of the 515 nm PL CdSeS/ZnS (core/shell) QDs as a function of [**2**] (0, 100, 500, and 1000 μM).

Emission decays in the absence of quencher and in the presence of 500 μM of each quencher are displayed in Figures 6

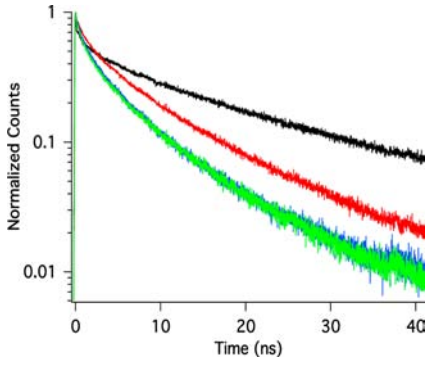

Figure 6. PL decay for the 474 nm PL QDs in the absence of quencher (black) and in the presence of 500 μM of **3** (green), **2** (blue), and **1** (red). The curves for **2** and **3** overlay.

and 7. In each case, the TRPL was best fit numerically with three exponentials (Figures S-14 and S-15, SI). For the 474 nm PL QDs, the fit gave lifetimes of 73 ps and 1.4 and 15.1 ns, while for the 515 nm PL QDs, this gave lifetimes of 0.43, 2.4, and 14.8 ns, with the amplitude of the third component being largest in both cases (Table 3). The 73 ps lifetime in the first case was close to the instrumental response time.

When the Cr(III) compounds were present, there were distinct changes in the decay curves, dependent on the nature of the Cr(III) cation. Decay rates increased in the presence of different q with the largest impact being on the longer lifetime components, namely, those that contribute the most to overall emission intensity under steady state excitation. Burda et al. reported effects on very short lifetime components in the picosecond transient absorption (TA) dynamics of CdSe QDs

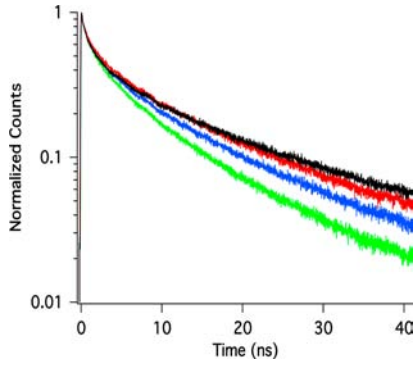

Figure 7. PL decay for the 515 nm PL QDs in the absence of quencher (black) and in the presence of 500 μM of **1** (red), **2** (blue), and **3** (green).

Table 3. Calculated Lifetimes and Amplitudes Using a Triple Exponential Fit Function for the Time-Resolved PL Decay from the 474 and 515 nm PL QDs in the Presence of 500 μM of Each Quencher

amplitudes (A_i) and lifetimes (τ_i)	QD	QD + 500 μM **1**	QD + 500 μM **2**	QD + 500 μM **3**
474 nm PL QDs				
A_1	0.26	0.26[a]	0.26[a]	0.26[a]
τ_1 (ns)	0.073	0.073[a]	0.073[a]	0.073[a]
A_2	0.24	0.30	0.35	0.36
τ_2 (ns)	1.4	1.4	1.3	1.2
A_3	0.50	0.45	0.39	0.39
τ_3 (ns)	15.1	9.2	7.0	7.2
515 nm PL QDs				
A_1	0.31	0.28	0.30	0.30
τ_1 (ns)	0.43	0.56	0.50	0.47
A_2	0.30	0.26	0.29	0.31
τ_2 (ns)	2.4	2.9	2.6	2.6
A_3	0.37	0.41	0.39	0.38
τ_3 (ns)	14.8	14.1	12.7	10.7

[a] A_1 and τ_1 were not allowed to vary.

in the presence of phthalocyanines.[26] However, ultrafast TA studies in this laboratory showed no obvious quenching of the short-lifetime components of the 515 or 474 nm PL QDs by Cr(III) quenchers used (data not shown), so there does not appear to be significant effects on short-lived states in the present studies.

For the 474 nm PL QDs, the numerical fits displayed little quencher-induced change in τ_2. However, there was a distinct pattern to changes in τ_3, which decreased from 15.1 ns with no quencher to 9.2, 7.0, and 7.2 ns, respectively, in 500 μM solutions of **1**, **2**, and **3**. (The variation in the amplitudes A_2 and A_3, which should remain nearly constant, may be an artifact from holding the first decay constant.) For the larger QDs, the A_i values varied less, and the τ_3 values showed systematic progression from 14.8 ns in the absence of quencher to 14.1, 12.7, and 10.7 ns in the presence of **1**, **2**, and **3**, respectively, consistent with the increase in $J(\lambda)$.

In the third experiment, the effect of quencher concentration on the emission decay from 515 nm PL core/shell QDs in solution was probed using the varying concentrations of **2** (Figure 8). Fitting the data with a triple exponential showed τ_1 and τ_2 to be essentially constant but τ_3 to decrease progressively with increasing [**2**] giving values of 14.8, 14.0, 12.7, and 11.9 ns for 0, 100, 500, and 1000 μM **2**, respectively.

dx.doi.org/10.1021/ja300771w | J. Am. Chem. Soc. 2012, 134, 13266−13275

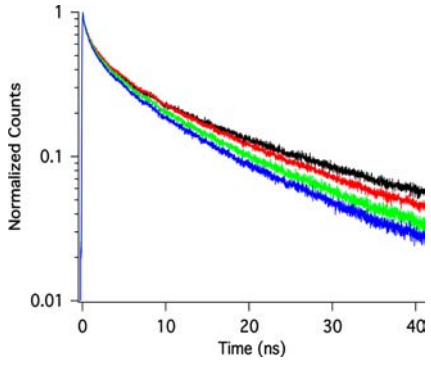

Figure 8. Normalized PL decay for the 515 nm PL QDs in the absence of quencher (black) and in the presence of varying concentrations of **2** (100 μM (red), 500 μM (green), and 1000 μM (blue). As expected, increasing concentration of **2** led to faster PL decay.

With regard to the model discussed above, the assumption that the excited state dynamics of these water-soluble core/shell QD preparations each display a single lifetime is clearly incorrect. Nonetheless, following the literature reports,[27] the slowest component of PL transients in colloidal II–VI QDs can be attributed to the radiative decay of the exciton, whereas faster transient processes (τ < 1 ns) are associated with the rapid trapping of charge carriers.[21b,c] It is this slower component that is quenched by the Cr(III) complexes while the latter are little affected, as demonstrated by transient PL and absorption measurements. This is consistent with FRET-based mechanism for quenching the QD excited states rather than a charge transfer mechanism. Furthermore, the bulk of the integrated emission intensity under steady state PL experiments is due to this longest-lived component, which also displays the largest amplitude. Thus, we can utilize the effects of the different quenchers on τ_3 to evaluate the relationship between spectral overlap and k_q.

If we use the relationship, $n = m(1 - e^{-b[q]})$ to estimate n, then the individual k_q values for **1**, **2**, and **3**, and the QD in question can be calculated from the relationship

$$\tau^0/\tau = 1 + \tau^0 n k_q \quad (8)$$

The numerical data shown in Table 4 were generated from this equation for TRPL experiments with the two sets of QDs with 500 μM quencher. The relative $k_q(i)$ values follow the trend shown in the steady state emission studies as expected from the conclusion that the τ_3 component dominates the integrated emission. A similar treatment of the data from Figure 7 appears in Table S-1 (SI). Notably, the $k_q(i)$ values calculated in this manner are all rather small, especially for the 515 nm PL QDs. Thus, significant quenching is achieved only because of the large number of individual Cr(III) cations assembled on the surface. In viewing this treatment, however, it should be noted that the estimated values of n listed and subsequent $k_q(i)$ values are directly dependent on the above estimates of m, the number of the Cr(III) cations that assembled on the surface at saturation. As a consequence, while we are confident that the relative $k_q(i)$ values described by Table 4 are reasonably valid, the absolute $k_q(i)$ values are subject to more uncertainty.

Table 4. k_q Values for 1, 2, and 3 Calculated from $n = m(1 - e^{-b[q]})$ and Eq 8 for 500 μM Quencher and the Experimental Values of τ_3[a]

	τ_3 (ns)	est. n	$k_q(i)$ (s^{-1})	$k_q(i)$ (relative)[b]
515 nm PL QDs	14.8	0	–	–
q = **1**	14.1	50	0.67×10^5	1.0
q = **2**	12.7	51	2.2×10^5	3.2
q = **3**	10.7	65	4.0×10^5	5.9
474 nm PL QDs	15.1	0	–	–
q = **1**	9.2	47	0.90×10^6	1.0
q = **2**	7.0	45	1.7×10^6	1.9
q = **3**	7.2	39	1.9×10^6	2.1

[a] m estimated as described in the text as ~65 and ~81 for the 474 and 515 nm PL QDs, respectively. [b] Normalized to the value of $k_q(i)$ calculated for each set of QDs.

4. OVERVIEW AND SUMMARY

Nitric oxide release from the *O*-nitrito complex *trans*-Cr(cyclam)$(ONO)_2^+$ is photosensitized by water-soluble CdSe/ZnS and CdSeS/ZnS core/shell quantum dots. Furthermore, the extent of NO release parallels the quenching of the QD band-edge photoluminescence. These observations clearly point to a mechanism by which excitation of the QD is followed by energy transfer to Cr(III) cations electrostatically bound to the anionic surface of the nanoparticle. Notably, this mechanism is different from that proposed by Medintz et al. for the quenching of similar QDs by the ruthenium phenanthroline derivatives and by ferrocene, where a charge transfer mechanism is apparently functioning.[13a,b]

While we cannot definitively exclude charge transfer from playing some role in this system, an energy transfer mechanism is favored for several reasons. First, NO release from CrONO is an excited state process, and the photochemistry of CrONO in the presence of QDs is equivalent to that of CrONO alone. This suggests that the enhanced NO production in the presence of QDs is due to excited QD states accessing the quartet-excited state of CrONO (Scheme 4) via an energy transfer mechanism followed by internal conversion to the lowest-energy, reactive doublet state.[9c] Second, it was noted previously that **1**, which had no spectral overlap with the band-edge emission of a set of 570 nm PL CdSe/ZnS QDs, did not quench that emission but did quench the longer wavelength "trap" emission. This observation suggested that a charge transfer quenching mechanism was occurring between surface trap states and **1**. Examination of the relative oxidation potentials led to the conclusion that this must be occurring

Scheme 4. Jablonski-Style Diagram Showing Energy Transfer from QD to the Quartet Excited State of CrONO Followed by Intersystem Crossing to the Doublet Excited State, To Which Is Attributed the NO Labilization Pathway[9c]

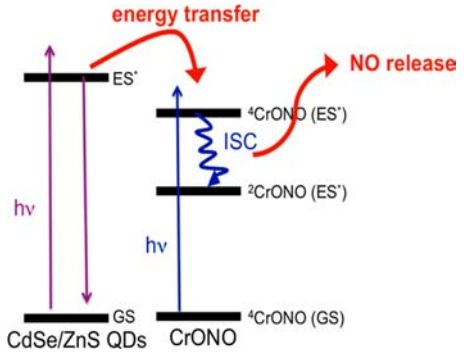

by QD to **1** hole transfer.[10b] However, oxidation of the Cr(III) metal center does not induce NO release from CrONO; therefore, the photoreaction must be induced by energy transfer. Notably, **1** does quench the band-edge PL from the smaller CdSe/ZnS core/shell QDs (PL λ_{max} 532 nm) and from the bluer emitting CdSeS/ZnS core/shell QDs (PL λ_{max} 474 and 515 nm).

The quenching of emission from different sized water-soluble CdSe/ZnS core/shell QDs by different *trans*-Cr(cyclam)$(X)_2^+$ salts shows a clear, although qualitative, correlation between the spectral overlap of donor PL and acceptor absorbance as expected for a FRET mechanism. A systematic comparison is provided here by using the homologous series of the photoinert *trans*-Cr$(N_4)(CN)_2^+$ salts as quenchers of the bluer emitting water-soluble, ternary CdSeS/ZnS core/shell QDs. Small perturbations of the equatorial tetraamine macrocycle N_4 ligands tune the LF absorption bands, hence the spectral overlap. Both the steady-state PL quenching and TRPL results show that the energy transfer rates track with the spectral overlap $J(\lambda)$ in agreement with a FRET energy transfer mechanism.

We also propose a model based on a static quenching mechanism facilitated by a dynamic equilibrium of Cr(III) cations electrostatically assembled at the anionic QD surfaces. This model defines the average number n of quenchers q bound to the surface. The total quenching rate constant is the product nk_q, where k_q is a function for the particular QD and quencher, whereas n is dependent on the quencher concentration $[q]$. On the basis of this model, it is shown that the serial equilibria leading to multiple q on the surface is operationally described by the relationship $n = m\,(1 - e^{-b[q]})$, where m is the estimated maximum number of q on the surface of a particular QD at limiting $[q]$. In the time-resolved PL results the longest lifetime component is significantly affected by the presence of various q, and we have used these temporal data to estimate quenching constants k_q that are further supportive of the FRET mechanism for energy transfer from QD to these Cr(III) centers. Therefore, we view spectral overlap as a guideline essential to developing supramolecular structures that effectively utilize QDs as sensitizers of photoreactions from such transition metal complexes.

■ ASSOCIATED CONTENT

Supporting Information

Detailed description of benchtop synthesis of water-soluble CdSeS/ZnS core/shell quantum dots and their characterization plus additional details on the photophysical properties of such materials in the absence and presence of Cr(III); an explanation of the calculation of the maximum number of cations that might occupy the QD surface in an electrostatic assembly. This material is available free of charge via the Internet at http://pubs.acs.org.

■ AUTHOR INFORMATION

Corresponding Author

ford@chem.ucsb.edu; paul.wagenknecht@furman.edu

Author Contributions

[#]P.T.B. and A.D.O. contributed equally to the research described.

Notes

The authors declare no competing financial interest.

■ ACKNOWLEDGMENTS

This work was supported by grants from the Chemistry Division of the U.S. National Science Foundation to P.C.F. (NSF-CHE-0749524 and NSF-CHE-1058794) and to P.S.W. (NSF-CHE-0709562). P.T.B. thanks the Corning Incorporated Foundation and the UCSB NSF Center for Nanotechnology in Society for fellowship support and A.D.O. thanks the NSF ConvEne IGERT program (NSF-DGE 0801627) for fellowship support. A.D.O. also thanks Dr. Hedi Mattoussi of the Naval Research Laboratory for advice in the synthesis of CdSe quantum dots. P.T.B. also thanks Dr. Niu Mutong and Professor Jinping Zhang from the Public Center for Characterization and Testing at the Suzhou Institute of Nanotech and Nanobionics (SINANO), Chinese Academy of Sciences, Suzhou, China for aid in TEM studies and the NSF PIRE-ECCI program at UCSB (NSF-OISE-05302680) for travel support to China. We thank the Molecular Foundry User Program and Dr. Delia Milliron, of the MF for assistance with WANDA optimization of the CdSeS synthesis. Work at the Molecular Foundry was supported by the Office of Science, Office of Basic Energy Sciences, of the U.S. Department of Energy under Contract No. DE-AC02-05CH1123. We also thank Richard Lewis of the UCSB Department of Chemistry and Biochemistry for his help with electrochemical measurements.

■ REFERENCES

(1) Ford, P. C. *Acc. Chem. Res.* **2008**, *41*, 190−200.

(2) Ford, P. C.; Bourassa, J.; Miranda, K.; Lee, B.; Lorkovic, I.; Boggs, S.; Kudo, S.; Laverman, L. *Coord. Chem. Rev.* **1998**, *171*, 185−202.

(3) Ostrowski, A. D.; Ford, P. C. *Dalton Trans.* **2009**, 10660−10669.

(4) Ignarro, L. J. *Nitric Oxide: Biology and Pathobiology*, 2nd ed.; Elsevier Inc.: Burlington, MA, 2010.

(5) Fang, F. C. *Nitric Oxide and Infection*; Kluwer Academic Publishers: New York, 1999.

(6) (a) Fukumura, D.; Kashiwagi, S.; Jain, R. K. *Nat. Rev. Cancer* **2006**, *6*, 521−534. (b) Hofseth, L. J.; Hussain, S. P.; Wogan, G. N.; Harris, C. C. *Free Radical Biol. Med.* **2003**, *34*, 955−968.

(7) (a) Wink, D. A.; Mitchell, J. B. *Free Radical Biol. Med.* **2003**, *34*, 951−954. (b) Wink, D. A.; Vodovotz, Y.; Laval, J.; Laval, F.; Dewhirst, M. W.; Mitchell, J. B. *Carcinogenesis* **1998**, *19*, 711−721.

(8) (a) Mitchell, J. B.; Wink, D. A.; DeGraff, W.; Gamson, J.; Keefer, L. K.; Krishna, M. C. *Cancer Res.* **1993**, *53*, 5845−5848. (b) Bourassa, J. L.; DeGraff, W.; Kudo, S.; Wink, D. A.; Mitchell, J. B.; Ford, P. C. *J. Am. Chem. Soc.* **1997**, *119*, 2853−2861.

(9) (a) De Leo, M.; Ford, P. C. *J. Am. Chem. Soc.* **1999**, *121*, 1980−1981. (b) Ostrowski, A. D.; Deakin, S. J.; Azhar, B.; Miller, T. W.; Franco, N.; Cherney, M. M.; Lee, A. J.; Burstyn, J. N.; Fukuto, J. M.; Megson, I. L.; Ford, P. C. *J. Med. Chem.* **2009**, *53*, 715−722. (c) Ostrowski, A. D.; Absalonson, R. O.; Leo, M. A. D.; Wu, G.; Pavlovich, J. G.; Adamson, J.; Azhar, B.; Iretskii, A. V.; Megson, I. L.; Ford, P. C. *Inorg. Chem.* **2011**, *50*, 4453−4462.

(10) (a) Neuman, D.; Ostrowski, A. D.; Absalonson, R. O.; Strouse, G. F.; Ford, P. C. *J. Am. Chem. Soc.* **2007**, *129*, 4146−4147. (b) Neuman, D.; Ostrowski, A. D.; Mikhailovsky, A. A.; Absalonson, R. O.; Strouse, G. F.; Ford, P. C. *J. Am. Chem. Soc.* **2008**, *130*, 168−175.

(11) (a) Alivisatos, A. P. *J. Phys. Chem.* **1996**, *100*, 13226−13239. (b) Leatherdale, C. A.; Woo, W.-K.; Mikulec, F. V.; Bawendi, M. G. *J. Phys. Chem. B.* **2002**, *106*, 7619−7622. (c) Schmelz, O.; Mews, A.; Basché, T.; Herrmann, A.; Müllen, K. *Langmuir* **2001**, *17*, 2861−2865. (d) Yu, W. W.; Qu, L.; Guo, W.; Peng, X. *Chem. Mater.* **2003**, *15*, 2854−2860. (e) Larson, Daniel R.; Zipfel, W. R.; Williams, R. M.; Clark, S. W.; Bruchez, M. P.; Wise, F. W.; Webb, W. W. *Science* **2003**, *300*, 1434−1436.

(12) (a) Medintz, I. L.; Mattoussi, H. *Phys. Chem. Chem. Phys.* **2009**, *11*, 17−45. (b) Rogach, A. L.; Klar, T. A.; Lupton, J. M.; Meijerink, A.; Feldmann, J. *J. Mater. Chem.* **2009**, *19*, 1208−1221. (c) Algar, W. R.; Tavares, A. J.; Krull, U. J. *Anal. Chim. Acta* **2010**, *673*, 1−25. (d) Becker, K.; Rogach, A. L.; Feldmann, J.; Talapin, D. V.; Lupton. *Appl. Phys. Lett.* **2009**, *95*, 143101. (e) Hsieh, J.; Ho, M.; Wu, P.; Chou, P.; Tsai, T.; Chi, Y. *Chem. Commun.* **2006**, 615−617. (f) Shi, L.; Hernandez, B.; Selke, M. *J. Am. Chem. Soc.* **2006**, *128*, 6278−6279. (g) Tsay, J. M.; Trzoss, M.; Shi, L.; Kong, X.; Selke, M.; Jung, M. E.; Weiss, S. *J. Am. Chem. Soc.* **2007**, *129*, 6865−6871. (h) Samia, A. C. S.; Chen, X.; Burda, C. *J. Am. Chem. Soc.* **2003**, *125*, 15736−15737.

(13) (a) Medintz, I. L.; Pons, T.; Trammell, S. A.; Grimes, A. F.; English, D. S.; Blanco-Canosa, J. B.; Dawson, P. E.; Mattoussi, H. *J. Am. Chem. Soc.* **2008**, *130*, 16745−16756. (b) Medintz, I. L.; Farrell, D.; Susumu, K.; Trammell, S. A.; Deschamps, J. R.; Brunel, F. M.; Dawson, P. E.; Mattoussi, H. *Anal. Chem.* **2009**, *81*, 4831−4839. (c) Blanco, N. G.; Maldonado, C. R.; Mareque-Rivas, J. C. *Chem. Commun.* **2009**, 5257−5259. (d) Gimenez, S.; Rogach, A. L.; Lutich, A. A.; Gross, D.; Poeschl, A.; Susha, A. S.; Mora-Sero, I.; Lana-Villarreal, T.; Bisquert. *J. Appl. Phys.* **2011**, *110*, 014314. (d) Koposov, A. Y.; Szymanski, P.; Cardolaccia, T.; Meyer, T. J.; Klimov, V. I.; Sykora, M. *Adv. Funct. Mater.* **2011**, *21*, 3159−3168. (e) Sykora, M.; Petruska, M. A.; Alstrum-Acevedo, J.; Bezel, I.; Meyer, T. J.; Klimov, V. I. *J. Am. Chem. Soc.* **2006**, *128*, 9984−9985. (f) Huang, J.; Stockwell, D.; Huang, Z.; Mohler, D. L.; Lian, T. *J. Am. Chem. Soc.* **2008**, *130*, 5632−5633.

(14) Lakowicz, J. R. *Principles of Fluorescence Spectroscopy*, 3rd ed.; Springer LLC: New York, NY, 2006.

(15) (a) Kane-Maguire, N. A. P.; Bennett, J. A.; Miller, P. K. *Inorg. Chim. Acta* **1983**, *76*, L123−L125. (b) Grisenti, D. L.; Smith, M. b.; Fang, L.; Bishop, N.; Wagenknecht, P. S. *Inorg. Chim. Acta* **2010**, *363*, 157−162. (c) Wagenknecht, P. S.; Ford, P. C. *Coord. Chem. Rev.* **2011**, *255*, 591−616.

(16) Clapp, A. R.; Goldman, E. R.; Mattoussi, H. *Nat. Protocols* **2006**, *1*, 1258−1266.

(17) (a) Al-Salim, N.; Young, A. G.; Tilley, R. D.; McQuillan, A. J.; Xia, J. *Chem. Mater.* **2007**, *19*, 5185−5193. (b) Chen, X.; Hutchison, J. L.; Dobson, P. J.; Wakefield, G. *Mater. Sci. Eng., B* **2010**, *166*, 14−18. (c) Chen, L.-Y.; Chen, C.-H.; Tseng, C.-H.; Lai, F.-L.; Hwang, B.-J. *Chem. Commun.* **2011**, *47*, 1592−1594.

(18) Chan, E. M.; Xu, C.; Mao, A. W.; Han, G.; Owen, J. S.; Cohen, B. E.; Milliron, D. J. *Nano Lett.* **2010**, *10*, 1874−1885.

(19) Crosby, G. A.; Demas, J. N. *J. Phys. Chem.* **1971**, *75*, 991−1024.

(20) Mikulec, F. V.; Kuno, M.; Bennati, M.; Hall, D. A.; Griffin, R. G.; Bawendi, M. G. *J. Am. Chem. Soc.* **2000**, *122*, 2532−2540.

(21) (a) We have no ready explanation for the drop in the net NO production and band-edge PL intensities at the shortest irradiation wavelengths (λ_{irr} < 300 nm). One possibility is suggested by observations by Kambhanpati and others (See refs 21b and 21c and references therein) that UV excitation of quantum dots leads to deactivation pathways that avoid the formation of the band-edge state, the state that is being probed by the photosensitized NO release. If this were the case, the quantum yields for photosensitized NO release should indeed decrease (however, it should be noted that this viewpoint is not universally held, see ref 21d). (b) Kambhampati, P. *J. Phys. Chem. C* **2011**, *115*, 22089−22109. (c) Kambhampati, P. *Acc. Chem. Res.* **2011**, *44*, 1−13. (d) Cruz, R. A.; Pilla, V.; Catunda, T. *J. Appl. Phys.* **2010**, *107*, 83504−7.

(22) (a) Jang, E.; Jun, S.; Pu, L. *Chem. Commun.* **2003**, 2964−2965. (b) Swafford, L. A.; Weigand, L. A.; Bowers, M. J.; McBride, J. R.; Rapaport, J. L.; Watt, T. L.; Dixit, S. K.; Feldman, L. C.; Rosenthal, S. J. *J. Am. Chem. Soc.* **2006**, *128*, 12299−12306.

(23) (a) Murray, C. B.; Norris, D. J.; Bawendi, M. G. *J. Am. Chem. Soc.* **1993**, *115*, 8706−8715. (b) Norris, D. J.; Sacra, A.; Murray, C. B.; Bawendi, M. G. *Phys. Rev. Lett.* **1994**, *72*, 2612.

(24) Hollingsworth, J. A.; Klimov, V. I. *Nanocrystal Quantum Dots*, 2nd ed.; CRC Press: Boca Raton, FL, 2010; p 16.

(25) (a) Dabbousi, B. O.; Rodriguez-Viejo, J.; Mikulec, F. V.; Heine, J. R.; Mattoussi, H.; Ober, R.; Jensen, K. F.; Bawendi, M. G. *J. Phys. Chem. B* **1997**, *101*, 9463−9475.

(26) (a) Dayal, S.; Królicki, R.; Lou, Y.; Qiu, X.; Berlin, J. C.; Kenney, M. E.; Burda, C. *Appl. Phys. B* **2006**, *84*, 309−315. (b) Dayal, S.; Lou, Y.; Samia, A. C. S.; Berlin, J. C.; Kenney, M. E.; Burda, C. *J. Am. Chem. Soc.* **2006**, *128*, 13974−13975.

(27) (a) Fisher, B. R.; Eisler, H.; Stott, N. E.; Bawendi, M. G. *J. Phys. Chem. B* **2004**, *108*, 143−148. (b) Klimov, V. I.; McBranch, D. W.; Leatherdale, C. A.; Bawendi, M. G. *Phys. Rev. B* **1999**, *60*, 13740−1374.